

IDENTIFYING AGN's BALMER-ABSORPTIONS AND STRATIFIED NLR KINEMATICS IN SDSS J112611.63+425246.4

J. Wang¹ and D. W. Xu¹

National Astronomical Observatories, Chinese Academy of Sciences
e-mail: wj@nao.cas.cn

October 28, 2014

ABSTRACT

Context. Balmer absorption is a rare phenomenon in active galactic nuclei (AGNs). So far, only seven Balmer-absorption AGNs have been reported in literature.

Aims. We here report the identification of SDSS J112611.63+425246 as a new Balmer-absorption AGN through our spectral analysis, and study the kinematics of its narrow emission-line region (NLR).

Methods. We model the continuum by a linear combination of a starlight component, a powerlaw from the central AGN and the emission from the FeII complex. After the subtraction of the modeled continuum, each emission/absorption line is profiled by a sum of multi Gaussian functions. All the line shifts are determined with respect to the modeled starlight component.

Results. By using the host starlight as a reference for the local system, both H α and H β show AGN's absorptions with a blueshift of $\sim 300\text{km s}^{-1}$. We identify a strong anti-correlation between the inferred velocity shifts and ionization potential for various narrow emission lines, which suggests a stratified NLR kinematics. A de-accelerated outflow is implied for the inner NLR gas, while an accelerated inflow for the outer NLR gas. This complicated NLR kinematics additionally implies that AGN's narrow emission lines, even for the low-ionized lines, might not be a reliable surrogate for the velocity of the local system.

Key words. galaxies: active — galaxies: peculiar — galaxies: individual(SDSS J112611.63+425246.4)

1. Introduction

The feedback from a central active galactic nucleus (AGN) is now believed to be a potential key ingredient in understanding the coevolution of the AGN and its host galaxy. A widely accepted scenario is that the growth of supermassive black hole (SMBH) regulates host star formation by sweeping out circum-nuclear gas (e.g., Silk & Rees 1998; Somerville et al. 2008; Hirschmann et al. 2013; Di Matteo et al. 2007; Fabian 1999; Granato et al. 2004; Croton et al. 2006).

The evidence of outflow from an AGN in various scales could be identified in multi-wavelength bands from radio to X-ray (see Veilleux et al. 2005 and Fabian 2012 for reviews). AGN's outflow could be diagnosed by the blueshifted absorption lines. Although the narrow absorption lines with width $\leq 500\text{km s}^{-1}$ are frequently identified in type I AGNs in UV and X-ray ($\sim 50\%$, e.g., Hamann & Sabra 2004), Balmer-absorption AGNs are still rare cases. So far, only seven Balmer-absorption AGNs are reported in literature, they are: NGC 4151 (Hutchings et al. 2002), SDSS J0839+3805 (Aoki et al. 2006), SDSS J1259+1213 (Hall 2007), SDSS J1029+4500 (Wang et al. 2008), SDSS 1723+5553 (Aoki 2010), LBQS 1206+1052 (Ji et al. 2012), and SDSS J2220+0109 (Ji et al. 2013). Because of their rarity, the identification of more Balmer-absorption AGNs is therefore essential for subsequent study of the nature of the AGN's Balmer absorption-line region (BAR). At first, recent studies point out that rigorous condition with high hydrogen column density of $\sim 10^{21-22}\text{cm}^{-2}$ is required to excite neutral hydrogen atoms to $n = 2$ shell by Ly α resonant pumping (e.g., Ji et al. 2012). Secondly, the Balmer absorption lines can be used as

a diagnostic for the kinematics of the natural gas around central AGNs.

In this paper, we report a detailed spectroscopic analysis for SDSS J112611.63+425246.4 (hereafter SDSS J1126+4252 for short)¹, which allows us to identify the object as a new Balmer-absorption AGN and to identify a stratified kinematics in its narrow emission-line region (NLR) with respect to the systematic velocity determined from the host galaxy.

2. Spectral Analysis

The optical spectrum of SDSS J1126+4252 is extracted when we carried out a systematic X-ray and optical spectral analysis on the XMM-Newton 2XMMi/SDSS-DR7 catalog that is originally crossmatched by Pineau et al (2011). The catalog contains a total of more than 30,000 X-ray point-like sources (with an X-ray position accuracy $\leq 5''$) that have a SDSS-DR7 optical counterpart with an identification probability larger than 90%. The spectrum of the object was taken by the SDSS dedicated 2.5m wide field telescope in February 27th, 2004.

The 1-Dimensional spectrum of the object is analyzed by the IRAF² package, including Galactic extinction correction, transformation to the rest frame, starlight component removal

¹ This object has been analyzed by Hu et al. (2008) in their large type-I AGN sample. The Balmer absorptions and starlight component were, however, not taken into account in their spectral modelings.

² IRAF is distributed by National Optical Astronomy Observatory, which is operated by the Association of Universities for Research in Astronomy, Inc., under cooperative agreement with the National Science Foundation.

and emission/absorption line profiling. We at first correct the Galactic extinction by the color excess $E(B - V)$ taken from the Schlegel, Finkbeiner, and Davies Galactic reddening map (Schlegel et al. 1998), by assuming an $R_V = 3.1$ extinction law of the Milky Way (Cardelli et al. 1989). The spectrum is then de-redshifted to its rest frame, along with the flux correction due to the relativity effect basing upon the measured redshift provided by the SDSS pipelines. The object has a nominal redshift of $z = 0.15592 \pm 0.00121$, which corresponds to a velocity uncertainty of 363 km s^{-1} .

The total light spectrum at the rest frame is displayed in Figure 1. It shows that there is non-negligible contamination from its host galaxy. To isolate the AGN's emission-line spectrum, we model the continuum by a linear combination of a power-law continuum, an FeII complex template and the seven eigen-spectra of starlight. The adopted FeII template is taken from Boroson & Green (1992). The eigenspectra were built from the standard single stellar population spectral library developed by Bruzual & Charlot (2003) through the principal component analysis (PCA) method (e.g., Wang & Wei 2008; Francis et al. 1992). An additional Galactic extinction curve with $R_V = 3.1$ is included in the modeling to account for the intrinsic extinction of the host galaxy. χ^2 minimizations are iteratively performed over the rest-frame wavelength range from 3700 to 7000 Å, except for the regions with strong emission lines. The line width of the FeII template and the velocity dispersion of the starlight are pre-determined through cross-correlation method before each iteration. The removal of the continuum is illustrated in Figure 1 as well.

The AGN's emission/absorption lines are subsequently modeled on the isolated line spectrum by using the SPECFIT task (Kriss 1994) in the IRAF package. The line modelings are schemed in the left and right panels in Figure 2 for the $H\alpha$ and $H\beta$ regions, respectively. The two narrow Balmer absorptions are marked by the vertical short lines in the figure. Each emission line is modeled by a free Gaussian function, except for the broad $H\alpha$ emission and the [OIII] doublet. Figure 2 clearly shows that a linear combination of two broad $H\alpha$ components are required to properly reproduce the observed line profile. We measure the FWHM of the total broad $H\alpha$ emission by the IRAF/SPLIT task from the residual profile that is obtained by subtracting the modeled narrow emission (i.e., $H\alpha$, [NII] $\lambda\lambda 6548, 6583$) and absorption lines from the observed profile. In addition to the narrow peak, a broad and blueshift component is necessary to model the slight blue wing of the [OIII] $\lambda 5007$ profile. The [OIII] $\lambda 4959$ ([NII] $\lambda 6548$) line profile is set to be the same as [OIII] $\lambda 5007$ ([NII] $\lambda 6583$). The intensity ratio of the [OIII] ([NII]) doublet is fixed to the theoretical value of 3. In total, the freedom in the χ^2 minimization is 21 and 15 for the $H\alpha$ and $H\beta$ regions, respectively.

3. Results and Discussions

The measured line properties are tabulated in Table 1. The reported flux of the $H\alpha$ broad emission (and the [OIII] $\lambda 5007$ line emission) is the sum of the two fitted components. The quoted line width and velocity shift is based on the fitted narrow peak for the [OIII] line. The flux of the FeII blends (FeII $\lambda 4570$) is measured in the rest-frame wavelength range from 4434 to 4684 Å, which results in a parameter of RFe of 0.64 ± 0.20 . RFe is defined as the flux ratio between the FeII $\lambda 4570$ and $H\beta$ broad component. All the reported line widths are not corrected for the intrinsic instrument resolution of $\sigma_{\text{inst}} \approx 65 \text{ km s}^{-1}$. Thanks to the evident contamination of the starlight in the integrated spectrum, we

emphasize that the reported line shifts are all calculated with respect to the modeled starlight component³: $\Delta v = \Delta v_{\text{line}} - \Delta v_{\text{host}}$, where Δv_{line} and Δv_{host} are the modeled velocity shifts with respect to the nominal redshift for a given emission/absorption line and for the host galaxy, respectively. A negative value of Δv corresponds to a blueshift, and a positive one to a redshift.

All the uncertainties reported in the table (except for the FWHM of $H\alpha_b$) only include the errors at 1σ significance level resulted from the χ^2 minimizations. The error of the FWHM of $H\alpha_b$ is obtained by a statistic on the multiple measurements by the IRAF/SPLIT task. A proper error propagation is taken into account in the reported uncertainties of Δv .

3.1. Balmer absorption lines

We argue that the observed blueshifted Balmer absorption lines are most likely resulted from an outflow from central engine, rather than from the host galaxy. In fact, the starlight component has been properly removed from the observed integral spectrum as described above. Moreover, the lack of a strong Balmer break enables us to exclude the case in which the observed Balmer absorptions are from a post-starburst galaxy with strong Balmer absorptions (e.g., Brotherton et al. 1999; Wang & Wei 2006). In interpretation of the Balmer absorptions in AGNs, the intrinsic EW depends on whether the absorbing gas covers the BLR or not (e.g., de Kool et al. 2001). The later scenario is favored in the object by comparing the measured Balmer absorption EW ratio to its theoretical value. In an absorption line without saturation, its EW could be related to its column density N as (Jenkins 1986):

$$EW_{\lambda} = \frac{\pi e^2 f \lambda^2 N}{m_e c^2} \quad (1)$$

where f is the oscillator strength. A theoretical $f\lambda$ value of 7.26 is therefore expected for the $H\alpha$ to $H\beta$ ratio, which is very close to the observed EW ratio of $EW(H\alpha)/EW(H\beta) = 7.38 \pm 4.32$ when both absorption lines are normalized with respect to the modeled AGN's continuum. On the contrary, the observed ratio is closed to 1 if both absorption lines are normalized to the corresponding broad emission line. This comparison therefore allows us to believe that the absorbing gas being responsible for the Balmer transitions is not saturated and fully covers the continuum source.

We further estimate the neutral hydrogen column density from Eq. (1). The inferred column densities of hydrogen at $n = 2$ shell from the $H\alpha$ and $H\beta$ absorption lines are $N_{\text{HI},2} = (1.2 \pm 0.5) \times 10^{14} \text{ cm}^{-2}$ and $(1.6 \pm 2.2) \times 10^{14} \text{ cm}^{-2}$, respectively. The neutral hydrogen column density could be derived from $N_{\text{HI}} \approx N_{\text{HI},1} + N_{\text{HI},2}$, where $N_{\text{HI},1}$ is the column density of hydrogen at $n = 1$ shell and is estimated by following Hall (2007):

$$\frac{N_{\text{HI},1}}{N_{\text{HI},2}} = \frac{1}{4\tau_{\text{Ly}\alpha}} e^{\frac{10.2\text{eV}}{kT}} \quad (2)$$

where $\tau_{\text{Ly}\alpha}$ is the optical depth at the center of the Ly α absorption. The depth $\tau_{\text{Ly}\alpha}$ could be inferred from the relationship $\tau_{\text{Ly}\alpha} = 0.12\tau_{\text{H}\alpha}(N_{\text{HI},1}/N_{\text{HI},2})$ (see Eq. (1) in Aoki 2010). Substituting this relationship into Eq (2) results in a relation

$$\frac{N_{\text{HI},1}}{N_{\text{HI},2}} = \frac{1.44}{\sqrt{\tau_{\text{H}\alpha}}} e^{\frac{5.1\text{eV}}{kT}} \quad (3)$$

³ Hu et al. (2008) uses the [OIII] $\lambda 5007$ line as a reference, and find that the [OII] emission line might be a more reliable reference than either [OIII] or $H\beta$. Our results are consistent with their measurements if the [OIII] line is used as a reference.

Taking $T = 7500\text{K}$ (Osterbrock & Ferland 2006) and $\tau_{\text{H}\alpha} = 1.69 \times 10^5 EW(\text{H}\alpha)/\lambda/b = 8.66$ (where b is the Doppler parameter of the absorption line after the correction of the intrinsic instrumental resolution), the inferred neutral hydrogen column density is $\sim 1.5 \times 10^{17} \text{ cm}^{-2}$.

3.2. UV and X-ray observations

SDSS J1126+4252 is particular weak and hard in UV and X-ray bands. The object is a common source in both second *XMM-Newton* serendipitous source catalog (XMMSSC) and *XMM-Newton* optical Monitor serendipitous UV source survey catalog (XMMOMSUS). Vagnetti et al. (2010) shows that the inferred specific luminosities at 2500\AA and 2keV are as low as $4.8 \times 10^{28} \text{ erg s}^{-1} \text{ Hz}^{-1}$ and $6.6 \times 10^{23} \text{ erg s}^{-1} \text{ Hz}^{-1}$, respectively. Its very hard X-ray spectrum could be additionally learned from the very large hardness ratios⁴: $HR3 = 0.52$ and $HR4 = 0.63$.

Ji et al. (2012, 2013) recently point out that a rigorous condition is required for the formation of Balmer absorptions. The absorptions are likely caused by Ly α resonant pumping in a partially ionized region with a high column density of $N_{\text{H}} \sim 10^{21-22} \text{ cm}^{-2}$. A heavy obscuration due to the required high column density is a possible explanation of the observed extremely weak and hard emission in both UV and X-ray.

3.3. Eddington ratio and SMBH mass

We estimate the SMBH mass M_{BH} in terms of its $\text{H}\alpha$ broad component according to the calibration in Greene & Ho (2007):

$$M_{\text{BH}} = 3.0_{-0.5}^{+0.6} \times 10^6 \left(\frac{L_{\text{H}\alpha}}{10^{42} \text{ erg s}^{-1}} \right)^{0.45 \pm 0.03} \left(\frac{\text{FWHM}_{\text{H}\alpha}}{1000 \text{ km s}^{-1}} \right)^{2.06 \pm 0.06} M_{\odot} \quad (4)$$

where $L_{\text{H}\alpha}$ is the intrinsic luminosity of the $\text{H}\alpha$ broad component corrected for the local extinction. The extinction is inferred from the narrow-line ratio $\text{H}\alpha/\text{H}\beta$, assuming the Balmer decrement for standard case B recombination and a Galactic extinction curve with $R_V = 3.1$. With the estimated M_{BH} , the Eddington ratio L/L_{Edd} (where $L_{\text{Edd}} = 1.26 \times 10^{38} M_{\text{BH}}/M_{\odot}$ is the Eddington luminosity) is obtained from a combination of the bolometric correction of $L_{\text{bol}} = 9\lambda L_{\lambda}(5100\text{\AA})$ (Kaspi et al. 2000) and the $L_{5100\text{\AA}} - L_{\text{H}\alpha}$ relation reported in Greene & Ho (2005)

$$\lambda L_{\lambda}(5100\text{\AA}) = 2.4 \times 10^{43} \left(\frac{L_{\text{H}\alpha}}{10^{42} \text{ erg s}^{-1}} \right)^{0.86} \text{ erg s}^{-1} \quad (5)$$

This luminosity relation has a rms scatter of 0.2dex around the best-fit line. The calculated M_{BH} and L/L_{Edd} are $\approx 1.8 \times 10^8 M_{\odot}$ and ≈ 0.06 , respectively. By combining the intrinsic scatters of the used relationships and the uncertainties derived from our line modelings, a proper error propagation returns 1σ uncertainties of 0.40dex and 0.45dex for the calculated M_{BH} and L/L_{Edd} .

We argue that the inferred M_{BH} from the broad $\text{H}\alpha$ emission agrees with the properties of the host galaxy. With the velocity dispersion of the host galaxy of $\sigma_{\star} \sim 270 \text{ km s}^{-1}$ obtained from our continuum modeling, the $M_{\text{BH}} - \sigma_{\star}$ relation of $\log(M_{\text{BH}}/M_{\odot}) = 8.13 + 4.02 \log(\sigma_{\star}/200 \text{ km s}^{-1})$ (Tremaine et al. 2004) yields a blackhole mass of $\log(M_{\text{BH}}/M_{\odot}) \sim 8.7$, which is highly consistent with the value estimated from the broad $\text{H}\alpha$ emission.

⁴ The hardness ratios are defined as $HR3 = (CR4 - CR3)/(CR4 + CR3)$ and $HR4 = (CR5 - CR4)/(CR5 + CR4)$, where $CR3$, $CR4$ and $CR5$ are the count rates in the energy bands 1-2, 2-4.5, 4.5-12keV, respectively.

3.4. Stratified NLR kinematics

The spectral analysis allows us to study the line shifts in SDSS J1126+4252 by using its host starlight component as a reference of the systematic velocity. One can see from Table 2 that all the low-ionized narrow emission lines show a redshift with respect to its host galaxy, while a blueshift could be identified in the high-ionized emission line $[\text{NeIII}]\lambda 3868$. It is interesting that the $[\text{OIII}]\lambda 5007$ emission line has a marginal blueshift of $\Delta v = -10 \pm 30 \text{ km s}^{-1}$.

A strong anti-correlation between the velocity shifts and ionization potential (IP) is shown in Figure 3. The velocity shift of the emitting gas of neutral hydrogen atom is taken from the measurement of narrow $\text{H}\alpha$ emission, both because the narrow $\text{H}\alpha$ and $\text{H}\beta$ emission show comparable velocity shifts and because of the higher signal-to-noise ratio of the narrow $\text{H}\alpha$ line. An average value of velocity shift is adopted in the figure for the $[\text{SII}]$ doublet. The best fit yields a relation of $\Delta v = (186.4 \pm 35.4) - (4.00 \pm 0.80)\text{IP}$. In fact, Komossa et al. (2008) propose a similar correlation between the line shift and IP in the narrow-line Seyfert 1 galaxies with large $[\text{OIII}]\lambda$ blueshift over 150 km s^{-1} .

Because the AGN's NLR gas is believed to be generally stratified in density and ionization potential (e.g., Filippenko & Halpern 1984; Filippenko 1985; De Robertis & Osterbrock 1986), our fitted relationship implies a complicate NLR kinematics in SDSS J1126+4252. A de-accelerated outflow is expected for the inner NLR gas, while an accelerated inflow for the outer NLR gas. The turnover of the radial velocity occurs at the $[\text{OIII}]\lambda 5007$ emission-line gas whose radial velocity shift with respect to the local system determined from the host starlight is very close to zero. Although the outflows from central AGNs in various scales have been frequently identified in AGNs (e.g., Komossa et al. 2008 and Fabian 2012 for a recent review), the inflows have already been revealed in a few of nearby AGNs through integrated field spectroscopic observations in both optical band and near-infrared (e.g., Fathi et al. 2005; Storchi-Bergmann et al. 2007; Riffel et al. 2008, 2013; Riffel & Storchi-Bergmann 2011). The observations reveal distinct kinematics for different emitting gas. The inflowing gas to the central active nucleus could be traced by the H_2 emission, and the outflowing gas by the $[\text{FeII}]$ emission, which is similar to the kinematics revealed in SDSS J1126+4252.

The implications described above is based on the scenario in which the detected NLR lines are seen in front of the central AGN. We here can not exclude an alternatively scenario in which these NLR lines are seen behind the central source. In this scenario, the obtained relationship implies a de-accelerated inflow for the inner NLR gas, and an accelerated outflow for the outer NLR gas.

Our spectral analysis indicates that in SDSS J1126+4252 all the narrow emission lines, except for the $[\text{OIII}]\lambda$, show non-negligible velocity shifts with respect to the local system determined from the host starlight. This fact puts forward a worry that AGN's narrow emission lines, even for the low-ionized lines, might be a non-reliable surrogate for the velocity of the local system. A large sample is needed to perform a further examination on the relationship between the velocity shifts of various narrow emission-lines and local system determined from host starlight in the feature.

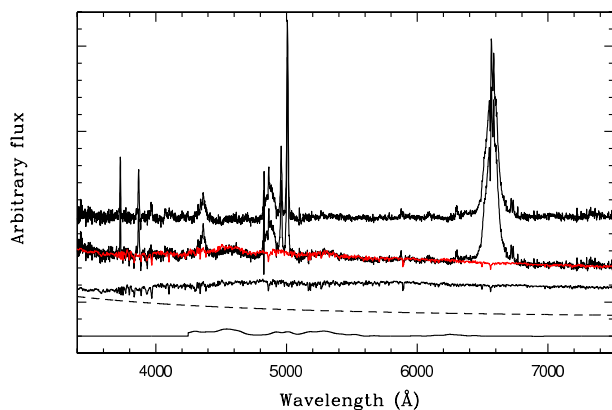


Fig. 1. Illustration of the modeling and removal of the continuum. The continuum-subtracted emission-line spectrum is shown by the top curve. Below the emission-line spectrum, the modeled continuum is overlaid by the red curve on the observed spectrum. The modeled continuum is obtained by a linear combination of a starlight component, a power-law continuum from the AGN and the emission from the FeII complex, which are displayed in ordinal below the observed spectrum. All the spectra are shifted vertically by an arbitrary amount for visibility.

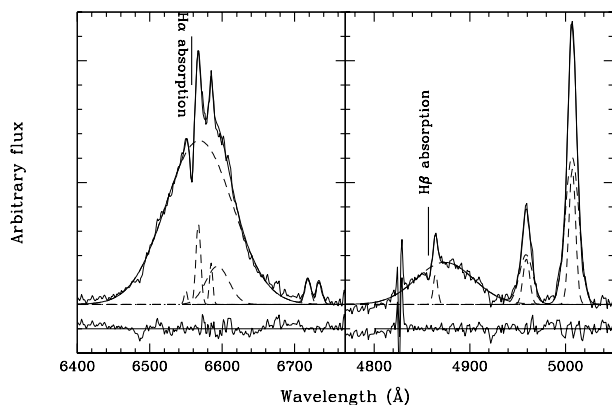


Fig. 2. Line profile modelings by a sum of a set of Gaussian components for the H α (left panel) and H β (right panel) regions. The blueshifted Balmer absorptions are marked by the short vertical lines. In each panel, the observed and modeled line profiles are plotted by the light and heavy solid lines, respectively. Each Gaussian component in emission is shown by a dashed line. The sub-panel underneath each line spectrum presents the residuals between the observed and modeled profiles.

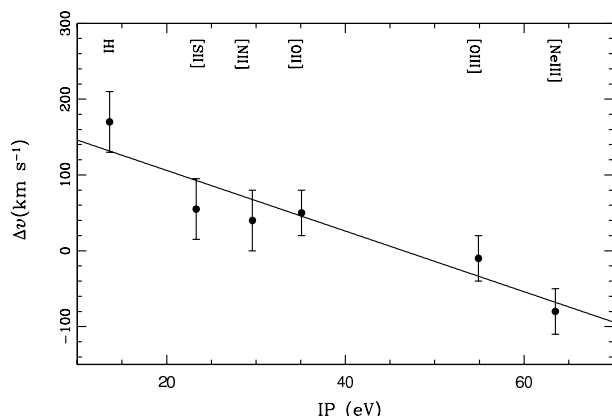


Fig. 3. Correlation between velocity shifts and ionization potential (IP). A positive velocity denotes a redshift, and a negative one a blueshift. The best fit line is over plotted by the solid line.

Table 1. Spectral properties of SDSS J1126+4252

Line	Emission		
	Flux $10^{-15} \text{ erg s}^{-1} \text{ cm}^{-2}$	FWHM km s^{-1}	Δv km s^{-1}
(1)	(2)	(3)	(4)
[OII] λ 3727 .	2.3 ± 0.2	520 ± 40	50 ± 30
[NeIII] λ 3868	2.6 ± 0.2	710 ± 50	-80 ± 30
FeII λ 4570 ..	8.3 ± 0.3	$\sim 3 \times 10^3$	100 ± 150
H β_n	0.7 ± 0.5	340 ± 250	150 ± 80
H β_b	13.0 ± 1.1	4350 ± 230	750 ± 30
[OIII] λ 5007.	15.8 ± 2.9	500 ± 90	-10 ± 30
H α_n	2.7 ± 1.1	350 ± 110	170 ± 40
H α_b	84.3 ± 2.8	4640.0 ± 70
[NII] λ 6583 .	1.0 ± 0.6	240 ± 120	40 ± 40
[SII] λ 6716..	1.1 ± 0.1	440 ± 40	50 ± 30
[SII] λ 6731..	1.0 ± 0.1	440 ± 40	60 ± 30
Absorption			
H β	28.8 ± 11.1	290 ± 540	-300 ± 70
H α	3.9 ± 5.6	210 ± 70	-250 ± 40

4. Conclusions

Detailed spectral analysis is performed on SDSS J11261.63+425246.4, which allows us to identify the object as a new Balmer-absorption AGN. Using the modeled host starlight as the reference of the local system, a stratified kinematics is identified in the NLR of the object, i.e., a strong anti-correlation between the inferred velocity shifts and ionization potentials. The revealed relationship implies a de-accelerated outflow stream for its inner NLR gas, and an accelerated inflow stream for its outer NLR gas.

Acknowledgements. The authors thank Profs. Todd A. Boroson and Richard F. Green for providing the optical FeII template. This research has made use of the SDSS archive data that are created and distributed by the Alfred P. Sloan Foundation. JW is supported by the National Natural Science Foundation of China (grant No. 11473036). DWX is supported by the National Natural Science Foundation of China under grant No. 11273027.

References

- Aoki, K. 2010, PASJ, 62, 1333
- Aoki, K., Iwata, I., Ohta, K., Ando, M., Akiyama, M., & Tamura, N. 2006, ApJ, 651, 84
- Boroson, T. A., & Green, R. F. 1992, ApJS, 80, 109
- Brotherton, M. S., et al. 1999, ApJ, 520, 87
- Bruzual, G., & Charlot, S. 2003, MNRAS, 344, 1000
- Cardelli, J. A., Clayton, G. C., & Mathis, J. S. 1989, ApJ, 345, 245
- Croton, D. J., Springel, V., White, S. D. M., et al. 2006, MNRAS, 365, 11
- de Kool, M., Arav, N., Becker, R. H., et al. 2001, ApJ, 548, 609
- De Robertis, M. M., & Osterbrock, D. E. 1986, ApJ, 301, 727
- Di Matteo, P., Combes, F., Melchior, A.-L., & Semelin, B. 2007, A&A, 468, 61
- Fabian, A. C. 1999, MNRAS, 308, L39
- Fabian, A. C. 2012, ARA&A, 50, 455
- Fathi, K., et al. 2006, ApJL, 641, 25
- Filippenko, A. V. 1985, ApJ, 289, 475
- Filippenko, A. V. & Halpern, J. P. 1984, ApJ, 285, 458
- Francis, P. J., Hewett, P. C., Foltz, C. B., & Chaffee, F. H. 1992, ApJ, 398, 476
- Granato, G. L., De Zotti, G., Silva, L., Bressan, A., & Danese, L. 2004, ApJ, 600, 580
- Greene, J. E., & Ho, L. C. 2005, ApJ, 630, 122
- Greene, J. E., & Ho, L. C. 2007, ApJ, 670, 92
- Hall, P. B. 2007, AJ, 133, 1271
- Hamann, F., & Sabra, B. 2004, ASPC, 311, 203
- Hu, C., Wang, J. M., Ho, L. C., Chen, Y. M., Zhang, H. T., Bian, W. H., & Xue, S. J. 2008, ApJ, 687, 78
- Hutchings, J. B., Crenshaw, D. M., Kraemer, S. B., Gabel, J. R., Kaiser, M. E., Weistrop, D., & Gull, T. R. 2002, AJ, 124, 2543

- Hirschmann, M., et al. 2013, MNRAS, 436, 2929
- Jenkins, E. B. 1986, ApJ, 304, 739
- Ji, T., Wang, T -G., Zhou, H -Y., & Wang, H -Y. 2012, RAA, 12, 369
- Ji, T., Zhou, H -Y., Wang, T -G., & Wang, H -Y. 2013, ChA&A, 37, 17
- Kaspi, S., et al. 2000, ApJ, 533, 631
- Komossa, S., Xu, D., Zhou, H., & Storch-Bergmann, T. 2008, ApJ, 680, 926
- Kriss, G. 1994, Adass, 3, 43
- Osterbrock, D. E., & Ferland, G. J. 2006, Astrophysics of Gaseous Nebulae and Active Galactic Nuclei, 2nd edition.
- Pineau, F.-X., Motch, C., Carrera, F., et al. 2011, A&A, 527, 126
- Riffel, R. A., & Storch-Bergmann, T. 2011, MNRAS, 417, 2752
- Riffel, R. A., Storch-Bergmann, T., Winge, C. 2013, MNRAS, 430, 2249
- Riffel, R. A., Storch-Bergmann, T., Winge, C., McGregor, P. J., Beck, T., & Schmitt, H. 2008, MNRAS, 385, 1129
- Schlegel, D., Finkbeiner, D. P., & Davis, M. 1998, ApJ, 500, 525
- Silk, J., & Rees, M. J. 1998, A&A, 331, L1
- Somerville, R. S., Hopkins, P. F., Cox, T. J., Robertson, B. E., & Hernquist, L. 2008, MNRAS, 391, 481
- Storch-Bergmann, T., et al. 2007, ApJ, 670, 959
- Tremaine, C. A., Heckman, T. M., Kauffmann, G., et al. 2004, ApJ, 613, 898
- Vagnetti, F., Turriziani, S., Trevese, D., & Antonucci, M. 2010, A&A, 519, 7
- Veilleux, S., Cecil, G., & Bland-Hawthorn, J. 2005, ARA&A, 43, 769
- Wang, J., & Wei, J. Y. 2006, ApJ, 648, 158
- Wang, J., & Wei, J. Y. 2008, ApJ, 679, 86
- Wang, T., Dai, H., & Zhou, H. 2008, ApJ, 674, 668